

# From aggressive driving to molecular motor traffic

Ambarish Kunwar<sup>†</sup>, Andreas Schadschneider<sup>‡</sup>, and Debashish Chowdhury<sup>†</sup>

<sup>†</sup>Department of Physics, Indian Institute of Technology, Kanpur 208016, India

<sup>‡</sup>Institut für Theoretische Physik, Universität zu Köln, Zùlpicher Str. 77, D-50937 Köln, Germany

**Abstract.** Motivated by recent experimental results for the step sizes of dynein motor proteins, we develop a cellular automata model for intra-cellular traffic of dynein motors incorporating special features of the hindrance-dependent step size of the individual motors. We begin by investigating the properties of the aggressive driving model (ADM), a simple cellular automata-based model of vehicular traffic, a unique feature of which is that it allows a natural extension to capture the essential features of dynein motor traffic. We first calculate several collective properties of the ADM, under both periodic and open boundary conditions, analytically using two different mean-field approaches as well as by carrying out computer simulations. Then we extend the ADM by incorporating the possibilities of attachment and detachment of motors on the track which is a common feature of a large class of motor proteins that are collectively referred to as cytoskeletal motors. The interplay of the boundary and bulk dynamics of attachment and detachment of the motors to the track gives rise a phase where high and low density phases separated by a stable domain wall coexist. We also compare and contrast our results with the model of Parmeggiani et. al. (Phys. Rev. Lett. **90**, 086601 (2003)) which can be regarded as a minimal model for traffic of a closely related family of motor proteins called kinesin. Finally, we compare the transportation efficiencies of dynein and kinesin motors over a range of values of the model parameters.

## 1. Introduction

Molecular motors are protein molecules that drive a wide range of intra-cellular activities including transport of molecular cargo [1, 2]. There are many similarities between collective molecular motor transport and vehicular traffic [3, 4]. In recent years non-equilibrium statistical mechanics has found unusual application in research on traffic flow of various different types of objects starting from objects as small as molecular motors to macroscopic objects like vehicles [5, 6, 3, 4]. Analytical as well as numerical techniques of the statistical physics are being used to understand rich variety of physical phenomena exhibited by traffic systems. Some of these phenomena, observed under different circumstances, include phase transitions, criticality and self-organized criticality, metastability and hysteresis, phase-segregation, etc.

A common modeling strategy is to represent the motile objects (e.g., a vehicle or a molecular motor) by a self-propelled particle, ignoring its structural details, and then treating the traffic as a system of interacting particles driven far from equilibrium. These models belong to a class of non-equilibrium systems called *driven-diffusive lattice gases* [7, 8, 9, 10]. In most of these traffic models the dynamics of the particles is formulated using the language of *cellular automata* (CA) [11].

To our knowledge, the first model for molecular motor traffic was formulated in 1968 in the context of collective movement of ribosomes on messenger RNA track [12, 13]. In recent years several groups have independently developed a class of minimal generic models for traffic of molecular motors which move on tracks that are filamentary proteins. All these models are essentially extensions of the totally asymmetric simple exclusion process (TASEP) [14, 7] which is one of the simplest models of driven diffusive lattice gas systems. In these models [15, 16, 17, 18, 19, 20] the molecular motors are represented by particles whereas the sites for the binding of the motors with the tracks are represented by a one-dimensional discrete lattice. Just as in TASEP, the motors are allowed to hop forward, with probability  $q$ , provided the site in front is empty. However, unlike TASEP, the particles can also get “attached” to an empty lattice site, with probability  $\omega_A$ , and “detached” from an occupied site, with probability  $\omega_D$  from any site except the end points. Parmeggiani et al. [15] demonstrated a novel phase where low and high density regimes, separated from each other by domain walls, coexist. They interpreted this spatial organization as traffic jam of molecular motors.

None of the models of molecular motor traffic mentioned above distinguish between kinesins and dyneins which form the two superfamilies of motor proteins that move on the same type of tracks, namely, microtubules. On the other hand, detailed experiments over the last two years have established that, in contrast to kinesins, dyneins can take steps of four different sizes depending on the opposing force or hindrance. One of the aims of this paper is to introduce a minimal model that distinguishes between these two features of kinesin and dynein motors.

In this paper we begin by investigating the aggressive driving model (ADM), a

stochastic CA model for traffic flow ‡ that is closely related to the Nagel-Schreckenberg (NaSch) model [22, 23]. One of the reasons for studying this model is that it allows natural extensions so as to capture the essential features of dynein motor traffic including the unique features of dynein stepping (which we shall explain in section 5.1). Besides, the ADM model is an interesting model of vehicular traffic in its own right and is also related to the Fukui-Ishibashi (FI) model [24]. However, in contrast to the FI model, it still shows spontaneous jam formation. We investigate the properties of the ADM by approximate analytical calculations as well as by computer simulations. Then, we use an extended version, which we refer to as the dynein traffic model (DTM), for a quantitative description of intra-cellular traffic of dynein motors.

The paper is organized as follows. In the next section we describe the ADM and the method of simulation. In section 3 we investigate the properties of the ADM with periodic boundary conditions and we describe the analytical theories for calculating its flow properties. We present a comparison of the ADM with NaSch model at the end of section 3. In section 4 we investigate the density profiles and phase diagram of the ADM with open boundary conditions. In section 5 we describe the experimentally observed hindrance-dependence of the step sizes of dynein motors and introduce the dynein traffic model (DTM). We present the results for the DTM with periodic boundary conditions in section 6 and those under open boundary conditions in section 7. Finally we summarize the main results and the conclusions in section 8.

## 2. The CA Model of Aggressive Driving

In the cellular automata model of aggressive driving a lane is represented by a one-dimensional lattice. The boundary conditions may be periodic or open. Each of the lattice sites represents a cell that can be either empty or occupied by at most one vehicle at a time. The speed  $V$  of each vehicle can take one of the allowed integer values  $V = 0, 1, 2, \dots, V_{\max}$ . Let  $x_n$  and  $V_n$  be the position and speed, respectively, of the  $n$ th vehicle. Then we define the (distance) headway of the  $n$ th vehicle at time  $t$  by  $d_n = x_{n+1} - x_n - 1$ , i.e. as the number of empty cells in front of this car. At each time step  $t \rightarrow t + 1$  the state of all vehicles on this 1-D lattice is updated in *parallel* according to the following rules:

*I: Acceleration:* If  $d_n \geq V_{\max}$  then  $V_n \rightarrow V_{\max}$  and if  $d_n < V_{\max}$  then  $V_n \rightarrow d_n$ , that is,  $V_n = \min(V_{\max}, d_n)$

*II: Randomization:* If  $V_n > 0$ , the speed of the  $n$ th vehicle is decreased randomly by one with probability  $p$ ; that is,  $V_n = \max(V_n - 1, 0)$  with probability  $p$

*III: Vehicle movement:* Each vehicle is moved forward so that  $x_n \rightarrow x_n + V_n$ .

Step *I* reflects the tendency of drivers to drive the vehicle as fast possible, without exceeding the maximum speed of the vehicle, and avoiding accidents between vehicles at the same time. Thus, if there is enough gap in front, vehicles in this model can accelerate to the maximum allowed velocity within one single timestep. This captures

‡ Originally the model was introduced in [21].

at least one type of aggressive driving and hence the name. The randomization in the step *II* takes into account the different behavioral patterns of the individual drivers, especially non-deterministic acceleration and over-reaction while slowing down.

As usual, the *flux* is defined to be the number of vehicles crossing a detector site per unit time. In the context of vehicular traffic, the most important quantity of interest is the so-called *fundamental diagram* which depicts the dependence of flux on the density of vehicles. The number of empty sites in between a pair of vehicles is usually taken as a measure of the corresponding *distance-headway*. The *time-headway* is defined as the time interval between the passage of two successive vehicles recorded by a detector placed at a fixed position on the highway. We have calculated all these characteristic quantities for the ADM and will present these results in the following sections.

Before presenting the results for the ADM, we would like to compare and contrast it with a few other well known models of vehicular traffic. In the NaSch model, the calculation of the speed of a vehicle at the next time step ( $t+1$ ) during the acceleration stage requires the knowledge of its speed at previous time step  $t$  and its speed after the deceleration stage depends on the available headway in front of it, whereas, in the aggressive driving model the calculation of the speed of a vehicle at next time step does not require any knowledge of its velocity at previous time step and depends only on the available headway in front of the vehicle. In contrast to the NaSch model it therefore has no velocity memory. From now onwards, we shall refer to this model as aggressive driving model (ADM).

This ADM differs from the Fukui-Ishibashi (FI) model [24] at Step *II* of the updating procedure. In the FI model the randomization is applied only to those vehicles whose final velocities become  $V_{\max}$  after the acceleration stage and, therefore, the FI model is unrealistic for normal traffic. Consequently, the FI model fails to capture overreactions at braking which are responsible for spontaneous jam formation (see e.g. [25]).

### 3. Results for ADM with periodic boundary conditions

#### 3.1. Numerical results of computer simulations

In the special case  $V_{\max} = 1$ , the ADM reduces to NaSch model [22] with  $V_{\max} = 1$ . In this limit the fundamental diagram is given by exact expression [23]

$$J = \frac{1}{2} \left[ 1 - \sqrt{1 - 4(1-p)c(1-c)} \right]. \quad (1)$$

The symmetry about  $c_* = 1/2$  in this fundamental diagram breaks down for all  $V_{\max} > 1$ . Fig. 1 shows the fundamental diagram of the ADM for different values of  $V_{\max}$  for fixed  $p = 0.25$  and  $p = 0.75$ . Fig. 2(a) and Fig. 2(b), show variation of flux and average speed, respectively, with  $c$  for different values of the braking probability  $p$  for fixed  $V_{\max} = 3$ .

For  $V_{\max} = 1$ , the fundamental diagram of ADM has a perfect particle-hole symmetry with a flow maximum at  $c = 0.5$ . However, as in the NaSch model, this

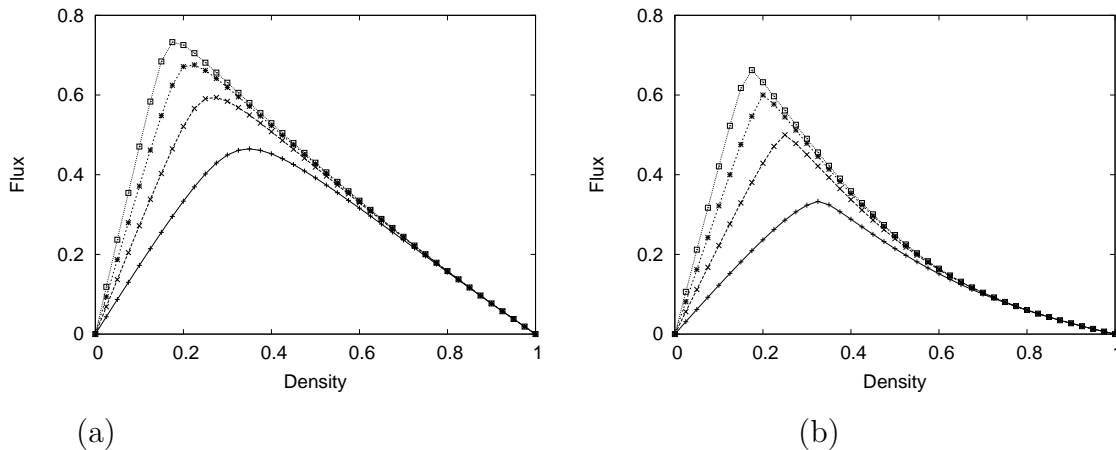


**Figure 1.** Fundamental diagram of the ADM for  $V_{\max} > 1$  corresponding to (a)  $p = 0.25$  and (b)  $p = 0.75$  respectively, obtained through computer simulations for  $V_{\max} = 2$  (+),  $V_{\max} = 3$  (x),  $V_{\max} = 4$  (\*), and  $V_{\max} = 5$  ( $\square$ ), respectively.

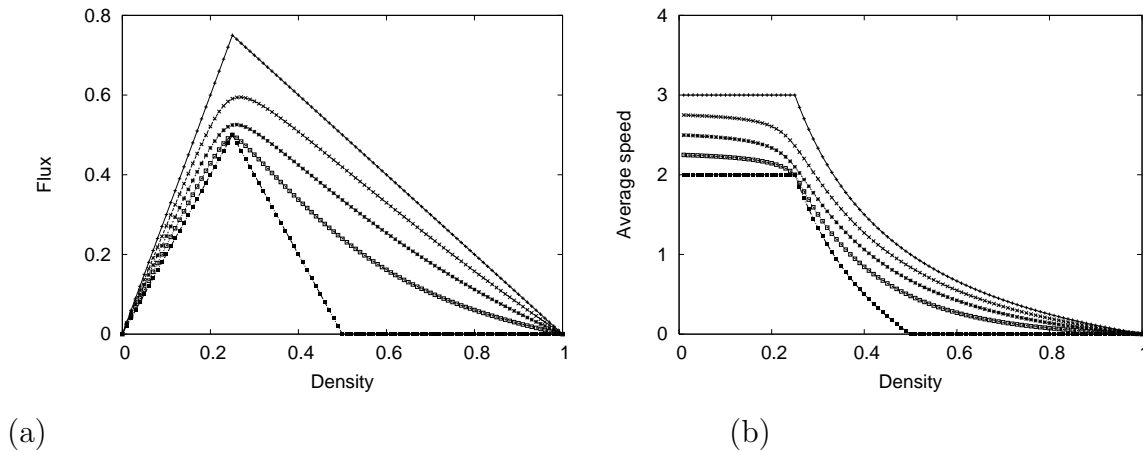


**Figure 2.** (a) Fundamental diagram and (b) density-dependence of the average speed of vehicles of the ADM with  $V_{\max} = 3$  for  $p = 0.0$  (+),  $p = 0.25$  (x),  $p = 0.50$  (\*),  $p = 0.75$  ( $\square$ ) and  $p = 1.0$  ( $\blacksquare$ ), respectively.

particle-hole symmetry breaks down for all  $V_{\max} > 1$  and the maximum shifts to lower densities with increasing  $V_{\max}$ . The system remains in the *free-flow* regime for densities on the left side of this maximum where the flux increases with increasing density. The densities on the right hand side of this maximum correspond to *congested flow* regime where flux starts decreasing with increasing density and finally vanishes at  $c = 1$ . For a given  $V_{\max}$ , the maximum value of the flux starts decreasing with increasing braking probability  $p$ . The fundamental diagram of the ADM shows unusual behavior in the deterministic limit  $p = 1$  where the flux vanishes at  $c = 0.5$  for all  $V_{\max} > 1$ . The reason for this unusual behavior will be explained in the following sections.

The *distance headway* is usually defined as the distance from a selected point on a vehicle to the same point on the corresponding lead vehicle (i.e., the next vehicle downstream). Since in our model all vehicles have the same length we can use the

number  $d_n$  of empty cells in front of vehicle  $n$  as a measure of the headway. In Fig. 3(a) we have shown the distribution  $P_n$  of the distance headway in ADM obtained from simulations.

At low densities the distance headway distribution shows a broad peak near  $n = V_{\max}$ . This corresponds to the free-flow regime where the cars are distributed almost homogeneously. In contrast, at larger densities the distribution exhibits two peaks one of which corresponds to free-flow regions whereas the new peak at  $n = 0$  corresponds to jammed regions on the highway. Finally, at sufficiently high densities the maximum of the probability distribution occurs only at  $n = 0$ . Thus, with increase of vehicle density, the compact cluster of jammed vehicles becomes larger while large headways are strongly suppressed.

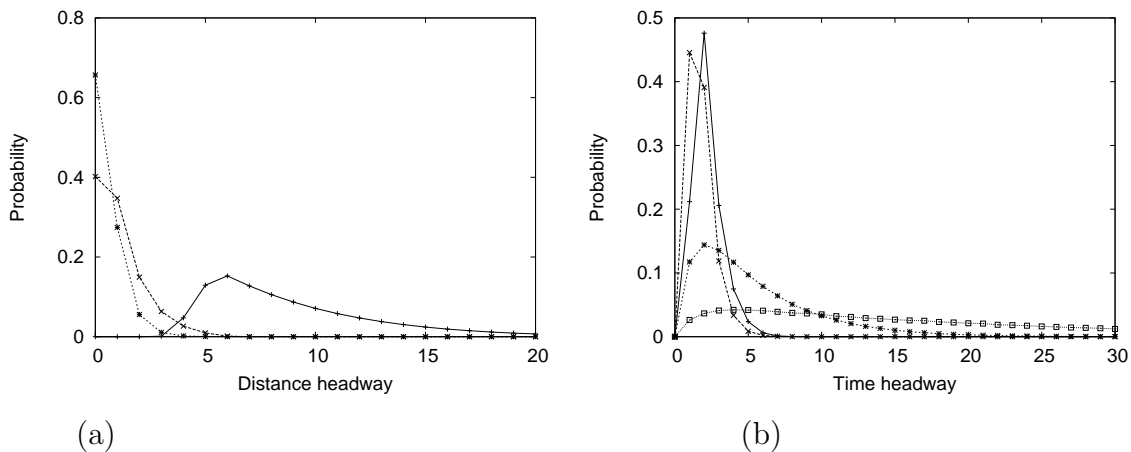


**Figure 3.** Steady-state distributions of (a) distance headways and (b) time headways for  $p = 0.5$  and  $V_{\max} = 5$  for densities  $c = 0.1(+)$ ,  $c = 0.3(\times)$ ,  $c = 0.7(*)$ ,  $c = 0.9(\square)$ .

The time headway distribution is determined by (a) the time interval between the departure from one site and arrival at the next site and (b) the waiting time at a given site; the latter depends not only on the hindrance from the vehicle in front but also on the randomization parameter  $p$ . Equivalently, the time-headway depends not only on the spatial distance-headway but also on the velocity of the vehicles.

A few typical time headway distributions  $P(\tau)$  in ADM are shown in Fig. 3(b) for a few different densities of the vehicles. At sufficiently low densities it shows a peak at  $\tau = 2$  as, because of the *parallel* updating scheme, minimum two time steps must elapse between the arrival of a vehicle at two successive sites even when it moves totally unhindered by any other vehicle. Since mean time headway is the inverse of the flux, it is expected to exhibit a minimum when plotted against the density. The trend of variation of the most probable time headway with increasing density is also similar, as can be seen also in Fig. 3. At low densities the peak is rather sharp and it becomes much broader at higher densities. Compared to the corresponding results for the NaSch model [26], large headways are suppressed in the ADM; this is caused by the possibility of large acceleration whereas in the NaSch only allowed acceleration is unity. The broader

distribution at higher densities arises from the longer waiting times at each site which is caused by the hindrance from the vehicle immediately in front.

### 3.2. Numerical and Exact Analytical Results for ADM in Limiting Cases

*3.2.1. Deterministic limit  $p=0$*  This stochastic model becomes deterministic in the limit  $p = 0$ . In this special case, the deterministic update rules of the model can be written as

$$V_n(t+1) = \min(V_{\max}, d_n) \quad (2)$$

$$x_n(t+1) = x_n(t) + V_n(t+1) \quad (3)$$

which leads to two types of steady states depending on density of vehicles [27]. At low densities, the system can self-organize so that  $d_n \geq V_{\max}$  for all  $n$  and, therefore every vehicle can move with  $V_{\max}$ , giving rise to the corresponding flux  $cV_{\max}$ . This steady state is, however, possible only if enough empty cells are available in front of every vehicle, i.e., for  $c \leq c_*^{\text{det}} = 1/(V_{\max} + 1)$  and the corresponding maximum flux is  $J_*^{\text{det}} = V_{\max}/(V_{\max} + 1)$ . On the other hand, for  $c > c_*^{\text{det}}$ ,  $d_n < V_{\max}$  and, therefore, the relevant steady states are characterized by  $V_n = d_n$ , i.e. flow is limited by density of holes. Since the average distance headway is  $1/c - 1$ , the fundamental diagram of the model in the deterministic limit  $p = 0$  is given by *exact* expression

$$J = \min[cV_{\max}, 1 - c]. \quad (4)$$

This is identical to the fundamental diagram of the NaSch model in the deterministic limit, despite the slightly different dynamics.

*3.2.2. Deterministic limit  $p = 1$*  As we discussed earlier in this paper that in the special case  $V_{\max} = 1$  the ADM reduces to NaSch model with  $V_{\max} = 1$  and hence in the deterministic limit  $p = 1$ ,  $J = 0$  for all densities  $c$  as expected. However, for  $V_{\max} > 1$ , the properties of the ADM with maximum allowed speed  $V_{\max}$  in the deterministic limit  $p = 1$  are not exactly identical to those of the same model with maximum allowed speed  $V_{\max} - 1$  and  $p = 0$ . If  $V_{\max} > 1$ , then, for  $c \geq 1/2$ , all initial states lead to  $J = 0$  because in the steady state system self-organizes itself in such a way that there is a maximum headway of one lattice site in front of each vehicle and hence speed of all vehicles becomes zero immediately after the randomization step (step *II* in update rules). However, for  $V_{\max} > 1$  and  $p = 1$ ,  $J \neq 0$  for all  $c < 1/2$ . The maximal attainable velocity for every vehicle in this limit becomes  $V_{\max} - 1$ . The fundamental diagram of ADM for  $V_{\max} > 1$  in the deterministic limit  $p = 1$  is given by *exact* expression

$$J = \begin{cases} \min[c(V_{\max} - 1), 1 - 2c] & \text{for } c \leq 1/2 \\ 0 & \text{for } c \geq 1/2. \end{cases} \quad (5)$$

This unusual behavior of the ADM is different from the corresponding behaviour in the NaSch model. In the deterministic limit  $p = 1$  of the NaSch model, irrespective of  $V_{\max}$

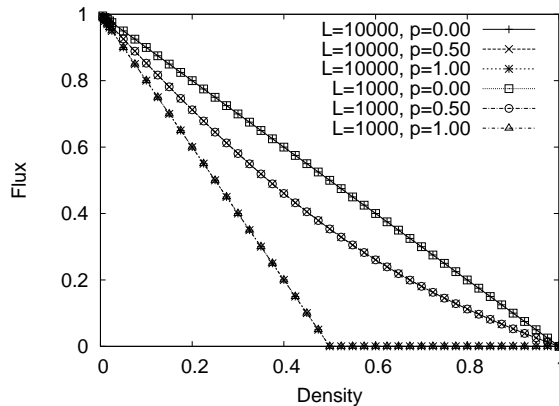


**Figure 4.** Fundamental diagram of the model with  $V_{\max} = L$  for system sizes  $L = 10000$  and  $L = 1000$  for typical values of  $p$ .

and  $c$ , all random initial states lead to  $J = 0$  [6], because a car which has velocity  $V = 0$  will never move again.

*3.2.3. Limit  $V_{\max} = \infty$*  There are several possible ways of extrapolating to this limit since only finite systems can be treated in computer simulations. We here investigate the case  $V_{\max} = L$ . The fundamental diagram of the model is plotted in Fig. 4 for different values of  $p$  in this limit. This fundamental diagram has a form quite different from that in the case of finite  $V_{\max}$ . The flow does not vanish in the limit  $c \rightarrow 0$  since already one single vehicle produces a finite value of flow,  $J(c \rightarrow 0) = 1$ .  $J(c)$  is a monotonically decreasing function of  $c$ . Another characteristic feature of this fundamental diagram is the absence of the characteristic plateau which is exhibited by the NaSch model with  $V_{\max} = \infty$  [28, 29].

### 3.3. Approximate analytical theories of ADM

In this section we will present the site-oriented mean-field (SOMF) and car-oriented mean-field (COMF) approaches for calculating the fundamental diagram of the ADM with periodic boundary conditions following the methods of [23] after a brief review of the earlier works done in this regard.

A SOMF theory was developed earlier for the FI model [30]. Starting with a microscopic relation for the updating rule, which describes the occupancy of each site on the lattice, a macroscopic time-evolution relation is obtained for the average speed of the vehicles by carrying out statistical averages. Mean field equations are obtained as the asymptotic limit of the evolution relation. This gives average vehicle speed in the long time limit as a function of the vehicle density.

A COMF theory for the FI model was developed in [31] starting with the basic equations which describe the time evolution of the headway in front of each car. By introducing the concept of inter-car spacing longer and shorter than the maximum



attainable velocity  $V_{\max}$ , the average speed of the vehicles has been obtained analytically as a function of car density in the asymptotic limit which corresponds to the steady state.

*3.3.1. Site-oriented Mean-field Theory of ADM* In the SOMF [23] approach,  $c_V(i, t)$  denotes the probability that there is a vehicle with speed  $V = 0, 1, 2, \dots, V_{\max}$  at site  $i$  at time step  $t$ . Then, obviously,  $c(i, t) = \sum_{j=0}^{V_{\max}} c_j(i, t)$  is the probability that the site  $i$  is occupied by a vehicle at the time step  $t$  (irrespective of its speed) and  $d(i, t) = 1 - c(i, t)$  is the corresponding probability that the site  $i$  is empty. Using the definition

$$J(c, p) = \sum_{V=1}^{V_{\max}} V c_V \quad (6)$$

for the flux  $J(c, p)$  one can determine the mean-field fundamental diagram for the given  $p$ , provided one can determine  $c_V$  in the mean-field approximation.

According to the update rules of the ADM, the time evolutions of the probabilities  $c_V(i, t)$  are given by the following equations:

*Step I: Acceleration* ( $t \rightarrow t_1$ )

$$c_0(i, t_1) = c(i, t)c(i+1, t) \quad (7)$$

$$c_V(i, t_1) = c(i+V+1, t) \prod_{j=1}^V d(i+j, t)c(i, t) \quad (0 < V < V_{\max}) \quad (8)$$

$$c_{V_{\max}}(i, t_1) = \prod_{j=1}^{V_{\max}} d(i+j, t)c(i, t) \quad (9)$$

*Step II: Randomization* ( $t_1 \rightarrow t_2$ )

$$c_0(i, t_2) = c_0(i, t_1) + pc_1(i, t_1) \quad (10)$$

$$c_V(i, t_2) = qc_V(i, t_1) + pc_{V+1}(i, t_1) \quad (0 < V < V_{\max}) \quad (11)$$

$$c_{V_{\max}}(i, t_2) = qc_{V_{\max}}(i, t_1) \quad (12)$$

*Step III: Movement of vehicles* ( $t_2 \rightarrow t+1$ )

$$c_V(i, t+1) = c_V(i-V, t_2) \quad (0 \leq V \leq V_{\max}) \quad (13)$$

Recall that ADM with  $V_{\max} = 1$  is identical to the NaSch model with  $V_{\max} = 1$ . Therefore, for nontrivial results of the ADM one must consider  $V_{\max} \geq 2$ . For  $V_{\max} = 2$ , the full SOMF equations read (with  $q = 1 - p$ )

$$c_0(i, t+1) = c(i, t)c(i+1, t) + pc(i+2, t)d(i+1, t)c(i, t) \quad (14)$$

$$c_1(i, t+1) = qc(i+1, t)d(i, t)c(i-1, t) + pd(i+1, t)d(i, t)c(i-1, t) \quad (15)$$

$$c_2(i, t+1) = qd(i, t)d(i-1, t)c(i-2, t) \quad (16)$$

In the steady state, i.e. for  $t \rightarrow \infty$ , the  $c_V(i, t)$  are independent of  $t$ . For periodic boundary conditions the system becomes homogeneous in the steady state and hence

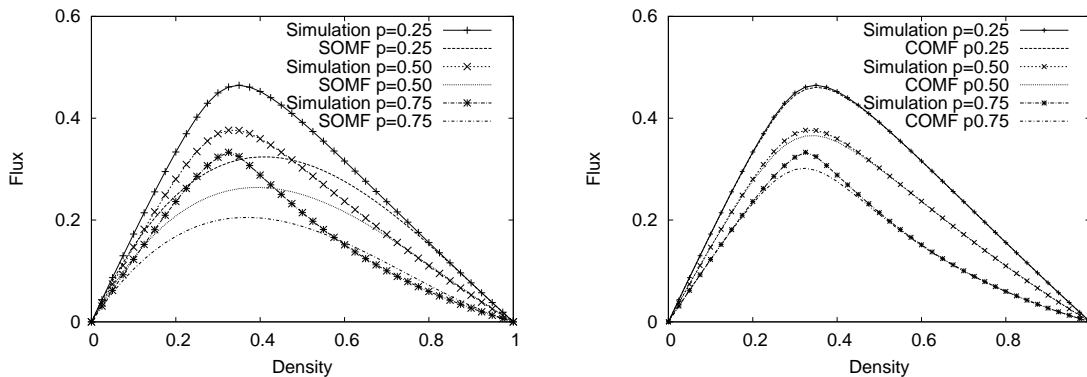


**Figure 5.** Comparison of site-oriented (left) and car-oriented (right) mean-field theory with results from computer simulation for  $V_{\max} = 2$ .

the  $i$ -dependence of  $c_V(i)$  also drops out. (14)-(16) then give  $c_V$  explicitly as a function of the density  $c$ . The steady state flux for  $V_{\max} = 2$  is then given by

$$J = c_1 + 2c_2 = c(1 - c)(2 - c - p) \quad (17)$$

The results obtained from the SOMF theory are plotted in Fig. 5(left) for a few values of  $p$  along with the corresponding numerical data from computer simulation. The agreement between the fundamental diagrams obtained from this simple SOMF theory and those obtained from computer simulations is quite poor because the important correlations between neighboring sites are neglected in this approach.

Interestingly, in contrast to the NaSch model [23], the fundamental diagram shows an inflection point at intermediate densities. This non-convexity of the flow-density relation becomes more pronounced for large values of the randomization  $p$ .

Asymptotically, for large densities  $c \approx 1$ , the flow in the ADM will be identical to that in the corresponding NaSch model, i.e.  $J \approx (1 - p)(1 - c)$ . However, in the NaSch model, and in many other traffic models, the flow at *any* density  $c$  can never exceed  $(1 - p)(1 - c)$ , the flow on the jammed branch. But, in contrast, because of the possibility of large acceleration of the vehicles in the ADM, the flow can far exceed the value  $(1 - p)(1 - c)$  at intermediate densities. Then, for obvious mathematical reasons, any smooth function with the asymptotic behaviour  $(1 - p)(1 - c)$  has to exhibit an inflection point.

In the NaSch model SOMF always systematically underestimates the true flux because of the effective particle-hole attraction [23]. Surprisingly, the same is not always true in the ADM (see e.g.  $p = 0.75$  in Fig. 5(left)). This indicates that the correlations in the ADM at intermediate densities are somewhat different from those in the NaSch case. Since now SOMF *overestimates* the flow over a range of density, this indicates the presence of effective particle-particle attraction, instead of particle-hole attraction in that regime. This is a consequence of the large accelerations of the vehicles which lead to a tendency towards particle-particle aggregation. This tendency becomes stronger at

large values of the randomization  $p$ , where fluctuations that reduce the velocity of a car temporarily become more likely.

In the next section we describe an improved mean field theory, namely car-oriented mean field theory, which takes into account certain correlations between the sites.

*3.3.2. Car-oriented Mean-field Theory of ADM* Here, we present the car-oriented mean-field (COMF) theory [32] of ADM with  $V_{\max} = 2$ . The central quantity in COMF theory is the probability  $P_n(t)$  to find at time  $t$  (exactly)  $n$  empty sites in front of a vehicle, i.e. the spatial headway distribution. The time evolution of the probabilities  $P_n(t)$  can conveniently be expressed through the probability  $g_j(t)$  ( $j = 0, 1, 2$ ) that a car moves  $j$  sites in the next time step.

In order to find the time evolution of the  $P_n(t)$  we first determine from which configurations at time  $t$  a given state at time  $t + 1$  could have evolved. Take for instance a car — called second car in the following — which has  $n \geq 4$  free sites in front, i.e. its distance to the next car ahead (called first car in the following) is  $n + 1$  sites. Since the velocity difference of the two cars is at most 2, a headway of  $n$  sites at time  $t + 1$  must have evolved from a headway of length  $n - 1$ ,  $n$ ,  $n + 1$  or  $n + 2$  in the previous time step. A headway of  $n - 1$  sites evolves into a headway of  $n$  sites only if the first car moves (with probability  $g_2(t)$ ) and the second car brakes in the randomization step (with probability  $p$ ), i.e. the total probability for this process is  $pg_2(t)P_{n-1}(t)$ . The headway will remain constant if the first car moves with probability  $g_1(t)$  and second car brakes with probability  $p$  (total probability for this process is  $pg_1(t)P_n(t)$ ) or the first car moves with probability  $g_2(t)$  and second car moves with probability  $q$  (total probability for this process is  $qg_2(t)P_n(t)$ ). Similarly, a headway of  $n + 1$  sites evolves into a headway of  $n$  sites if the first car does not move (probability  $g_0(t)$ ) and second car brakes with probability  $p$  (total probability being  $pg_0(t)P_{n+1}(t)$ ) or the first car moves with probability  $g_1(t)$  and second car moves with probability  $q$  (total probability for this process is  $qg_1(t)P_{n+1}(t)$ ). Finally, a headway of  $n + 2$  evolves into a headway of  $n$  only if the second car moves with probability  $q$  (total probability for this  $qg_0(t)P_{n+2}(t)$ ).

The special cases  $n = 0, 1, 2$  and  $3$  can be treated in an analogous fashion. In this way one obtains the time evolution of the probabilities as

$$P_0(t + 1) = g_0(t)P_0(t) + qg_0(t)[P_1(t) + P_2(t)], \quad (18)$$

$$P_1(t + 1) = g_1(t)P_0(t) + (pg_0(t) + qg_1(t))[P_1(t) + P_2(t)] + qg_0(t)P_3(t), \quad (19)$$

$$P_2(t + 1) = g_2(t)P_0(t) + (pg_1(t) + qg_2(t))[P_1(t) + P_2(t)] \\ + (pg_0(t) + qg_1(t))P_3(t) + qg_0(t)P_4(t), \quad (20)$$

$$P_3(t + 1) = pg_2(t)[P_1(t) + P_2(t)] + (pg_1(t) + qg_2(t))P_3(t) \\ + (pg_0(t) + qg_1(t))P_4(t) + qg_0(t)P_5(t), \quad (21)$$

$$P_n(t + 1) = pg_2(t)P_{n-1}(t) + (pg_1(t) + qg_2(t))P_n(t) \\ + (pg_0(t) + qg_1(t))P_{n+1}(t) + qg_0(t)P_{n+2}(t) \quad (n \geq 4) \quad (22)$$

A car will not move in next time step if there is no empty site in front of it (probability

$P_0(t)$ ) or if there is exactly one empty site in front of it and it decelerates in the randomization step 2 (probability  $pP_1(t)$ ). It will move one site if either there is exactly one empty site ahead and it does not decelerate (probability  $qP_1(t)$ ) or there are at least two empty sites in front, but the car decelerates in step 2 (probability  $p \sum_{n \geq 2} P_n(t)$ ). In all other cases it will move two sites. Therefore the probability  $g_j(t)$  that a car moves  $j$  sites in the next time step is given by

$$\begin{aligned} g_0(t) &= P_0(t) + pP_1(t) \\ g_1(t) &= qP_1(t) + p \sum_{n \geq 2} P_n(t) = p - pP_0(t) + (q - p)P_1(t) \\ g_2(t) &= q \sum_{n \geq 2} P_n(t) = q[1 - P_0(t) - P_1(t)] \end{aligned} \quad (23)$$

where we have used the normalization condition

$$\sum_{n \geq 0} P_n(t) = 1 \quad (24)$$

to rewrite the probabilities  $g_j(t)$  in terms of  $P_0(t)$ ,  $P_1(t)$ ,  $P_2(t)$  and  $P_3(t)$  only.

The probabilities can also be related to the density  $c = N/L$  of cars. Since each car which has the headway  $n$  to the next car one in front of it 'occupies'  $n + 1$  sites we have following relation:

$$\sum_{n \geq 0} (n + 1)P_n(t) = \frac{1}{c}. \quad (25)$$

Here we are mainly interested in the stationary state ( $t \rightarrow \infty$ ) with  $\lim_{t \rightarrow \infty} P_n(t) = P_n$ . In order to determine the probabilities in the stationary state we introduce the generating function

$$P(z) = \sum_{n=0}^{\infty} P_n z^{n+1} \quad (26)$$

After multiplying corresponding equation in [18-22] by  $z^{n+1}$  and summing over all equations one finds an explicit expression for the generating function,

$$P(z) = \frac{a_5 z^5 + a_4 z^4 + a_3 z^3 + a_2 z^2 + a_1 z}{-pg_2(z^2 - 2b_1 z + b_2)} \quad (27)$$

with

$$\begin{aligned} a_1 &= qg_0 P_0, & a_2 &= (g_0 + qg_1)P_0 + qg_0 P_1, \\ a_3 &= (g_1 + qg_2)P_0 + (pg_0 + qg_1)P_1, & a_4 &= g_2 P_0 + (pg_1 + qg_2)P_1, & a_5 &= pg_2 P_1, \\ b_1 &= \frac{qg_1 + g_0}{2pg_2}, & b_2 &= -\frac{qg_0}{pg_2}. \end{aligned} \quad (28)$$

Note that  $\sum_j a_j = (1 + q)P_0 + P_1$ . The denominator of  $P(z)$  has two zeros located at  $s_{\pm} = b_1 \pm \sqrt{b_1^2 - b_2}$  with  $|s_+| \geq 1$  and  $|s_-| \leq 1$ .

The normalization condition (24) is equivalent to  $P(1) = 1$  and is already satisfied by (27). The density relation implies  $P'(1) = \frac{1}{c}$ , where  $P'(z)$  denotes the

derivative of  $P(z)$ . In order to have  $0 \leq P_n \leq 1$  and  $\lim_{n \rightarrow \infty} P_n = 0$  the generation function must be analytic in the unit disc  $|z| \leq 1$ . Therefore the zero  $s_-$  of the denominator has to be cancelled by a corresponding zero of the numerator. The equation  $a_5 s_-^5 + a_4 s_-^4 + a_3 s_-^3 + a_2 s_-^2 + a_1 s_- = 0$  yields a relation between the variable  $P_0$  and  $P_1$  so that  $P(z)$  only depends on one free parameter, e.g.  $P_0$ . This parameter, in turn, is a function of the only physically relevant parameter, the density  $c$ , via  $P'(1) = \frac{1}{c}$ .

To obtain the fundamental diagram we have to calculate the flux. It is given by

$$J(c, p) = c[g_1 + 2g_2]. \quad (29)$$

In order to calculate the flux  $J(c, p)$  for a given set of  $c$  and  $p$  one has to solve the following two equations numerically.

$$a_5 s_-^5 + a_4 s_-^4 + a_3 s_-^3 + a_2 s_-^2 + a_1 s_- = 0 \quad (30)$$

and

$$P'(1) = \frac{1}{c} \quad (31)$$

where  $P'(z)$  denotes the derivative of  $P(z)$ . Eq. (31) can be written as

$$\frac{pg_2(2 - 2b_1) + (5a_5 + 4a_4 + 3a_3 + 2a_2 + a_1)}{pg_2(1 - 2b_1 + b_2)} + \frac{1}{c} = 0 \quad (32)$$

Eqs. (30) and (32) were solved numerically using function *FindRoot* of Mathematica5 by choosing the starting values for  $P_0$  and  $P_1$ .  $FindRoot[\{eqn_1, eqn_2, \dots\}, \{\{x_1, n_1\}, \{x_2, n_2\}, \dots\}]$  searches for a numerical solution to the simultaneous equations  $eqn_i$  starting with  $x_i = n_i$ . Values of  $P_0$  and  $P_1$  thus obtained for a given set of  $c$  and  $p$  are used to calculate the values of  $g_0$ ,  $g_1$  and  $g_2$ . Finally flux  $J$  is calculated using equation (29).

The results obtained from COMF are plotted in Fig. 5(right) for a few values of  $p$  along with the corresponding numerical data from computer simulation. Fundamental diagrams obtained from COMF show an excellent agreement with the numerical data in the limit  $p \rightarrow 0$ . Thus COMF can capture the important correlations much better than SOMF. Especially it is able to reproduce the occurrence of an inflection point at larger values of  $p$ . The small deviations are due to the fact that COMF neglects the correlations between the headways in front of successive vehicles.

### 3.4. Comparison of ADM with Nagel-Schreckenberg Model

In Fig. 6 we have plotted the fundamental diagram of the ADM with  $V_{\max} = 3$  and the average speed of vehicles against their density along with that of the NaSch model with  $V_{\max} = 3$  for a few values of  $p$ . In the absence of randomization, i.e. for  $p = 0$ , this model and the NaSch model give identical fundamental diagram and variation of average speed with density. In the presence of randomization, i.e.  $p \neq 0$ , the flow in the ADM is always larger than that of the corresponding NaSch model due to the faster acceleration. This difference is most pronounced at densities slightly beyond the maximum flow.

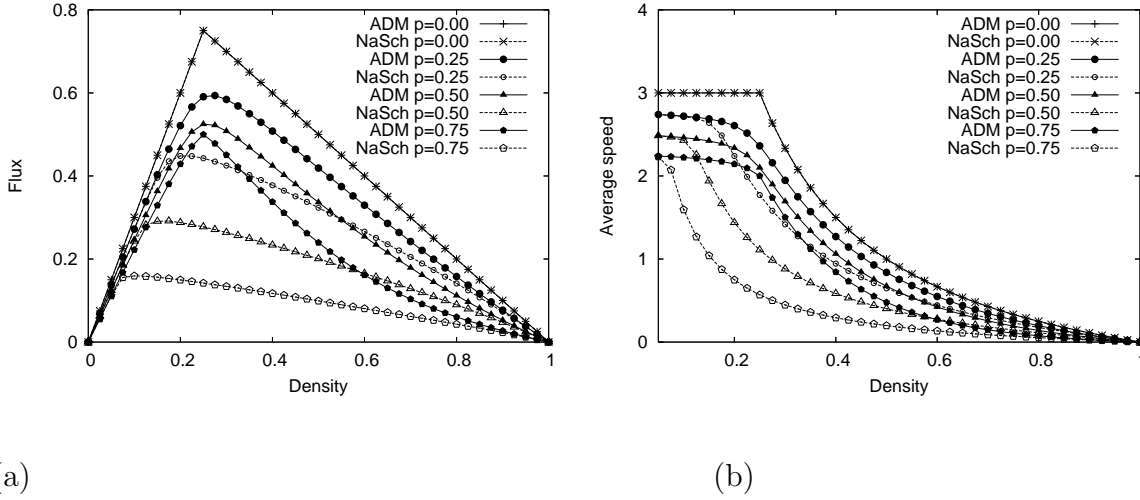


**Figure 6.** (a) The fundamental diagram of the model plotted along with the fundamental diagram of NaSch model for  $V_{\max} = 3$  for a few values of  $p$ . (b) Average speed of vehicles plotted against their densities for the model of aggressive driving along with the NaSch model for  $V_{\max} = 3$  for a few values of  $p$ .

#### 4. ADM with Open Boundary Conditions

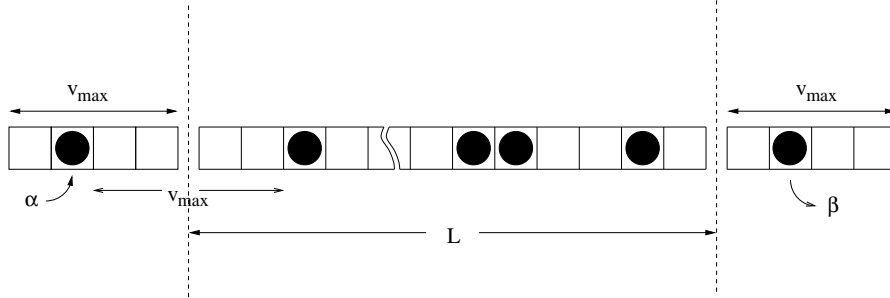


**Figure 7.** Schematic representation of the analyzed system with open boundary conditions. The main system consists of  $L$  cells. Vehicles move from left to right, and are represented by dark circles. The left boundary consists of mini system of  $V_{\max}$  cells. This left mini system is occupied by at most one vehicle with probability  $\alpha$ . Similarly the right boundary consists of a mini system of  $V_{\max}$  cells and particles are extracted from it with probability  $\beta$ . We shall represent each cell by a site on the lattice formed by these cells.

In this section we consider the ADM with open boundary conditions where vehicles move deterministically, i.e. with randomization probability  $p = 0$ .

A schematic representation of the analyzed system is shown in Fig. 7. Our main system consist of  $L$  cells. This main system is connected to two mini systems of length  $V_{\max}$  on each side [33]. This is done to provide a proper insertion and extraction strategy allowing us to investigate the whole spectrum of the possible states. The state of the mini system of the left boundary has to be updated every time step before the vehicles

of whole system. The update procedure consists of two steps. If any cell of the left mini system is occupied it has to be emptied first. Then a vehicle is inserted in the system with probability  $\alpha$ . The position of the inserted vehicle has to satisfy the following conditions: (i) The headway between the inserted vehicles in the mini system and the first vehicle in the main system is equal to  $V_{\max}$ , and (ii) the distance to the main system has to be minimum i.e. if there is no vehicle present in the main system within first  $V_{\max}$  cell then the rightmost cell of the left boundary is occupied. The right boundary consists of  $V_{\max}$  cells and vehicle are removed from these cells with probability  $\beta$ . These boundary conditions are capable of generating all flows observed in the case of periodic boundary conditions, including the maximal flow. From now onwards, we shall represent the cells by the sites of a lattice formed by the cells.

The above insertion and extraction scheme generates the maximum flow of the corresponding aggressive driving model with periodic boundary conditions for  $\alpha = \beta = 1$ , i.e.

$$J = \frac{V_{\max}}{V_{\max} + 1} \quad (\text{for } \alpha = \beta = 1). \quad (33)$$

#### 4.1. Density Profiles in the ADM

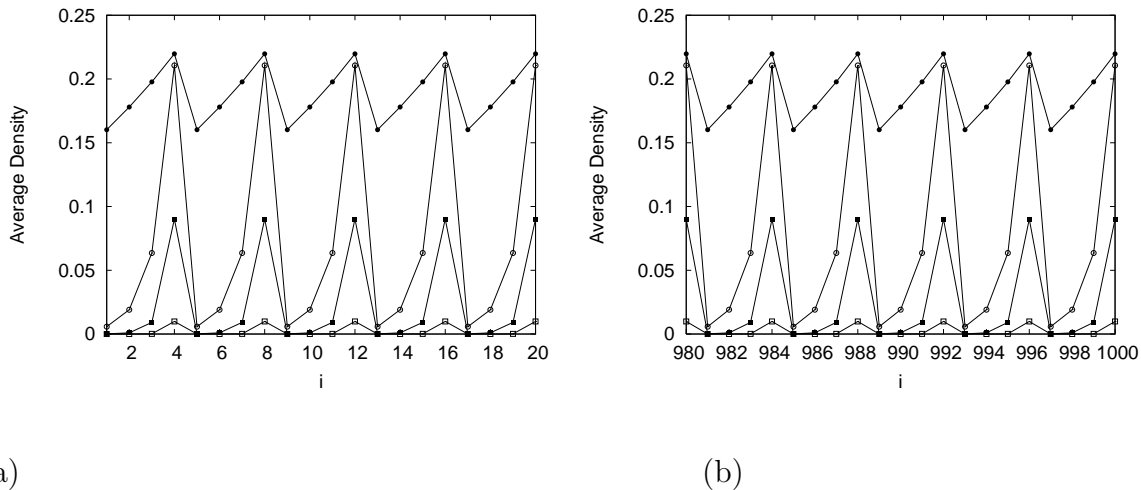


**Figure 8.** (a) Density profile at the beginning of the system; (b) Density profile at the end of the system  $V_{\max} = 4$  and  $L = 1000$ .  $\alpha=0.01$  and  $\beta=1.0$  ( $\square$ ),  $\alpha=0.1$  and  $\beta=1.0$  ( $\blacksquare$ ),  $\alpha=0.3$  and  $\beta=1.0$  ( $\circ$ ),  $\alpha=0.9$   $\beta=1.0$  ( $\bullet$ ).

The system is found in free flow regime for small  $\alpha$  and large  $\beta$ . In Fig. 8 we have shown density profiles at the beginning and the end of the system for  $V_{\max} = 4$  and  $L = 1000$  in the free flow regime. The density profile shows a periodic structure with a period of oscillation  $\Delta i = 4$ . For any arbitrary  $V_{\max}$ , we find that the period of this oscillating pattern  $\Delta i = V_{\max}$ . In order to understand this periodicity we first consider the density profile for very low injection rates and maximum extraction rate ( $\beta = 1$ ) (see Fig. 8).

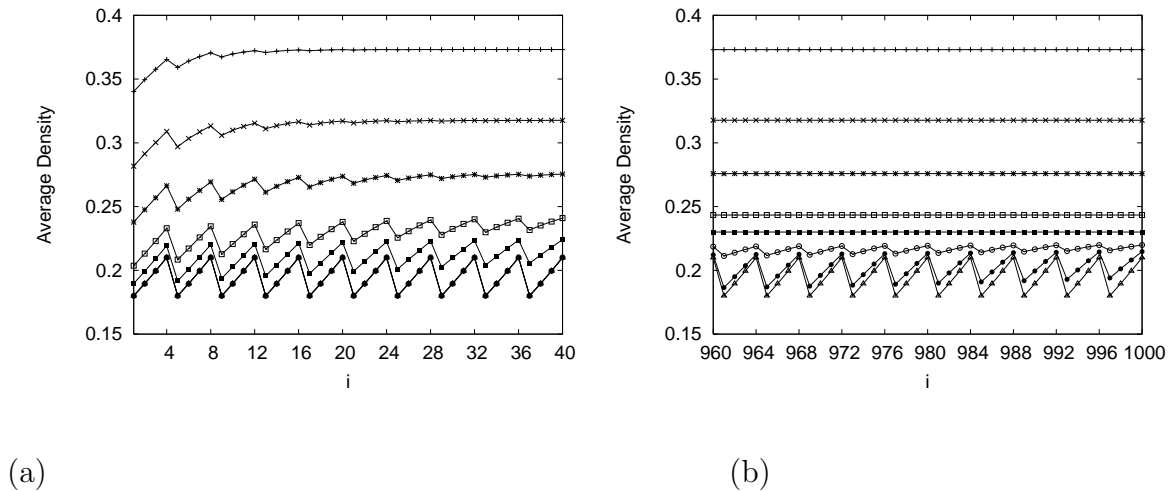


**Figure 9.** (a) Density profile at the beginning of the system (b) Density profile at the end of the system for  $V_{\max} = 4$  and  $L = 1000$ .  $\alpha=0.95$  and  $\beta=0.50$  (+),  $\alpha=0.95$  and  $\beta=0.60$  ( $\times$ ),  $\alpha=0.95$  and  $\beta=0.70$  (\*),  $\alpha=0.95$  and  $\beta=0.80$  ( $\square$ ),  $\alpha=0.95$  and  $\beta=0.85$  ( $\blacksquare$ ),  $\alpha=0.95$  and  $\beta=0.90$  (o),  $\alpha=0.95$  and  $\beta=0.95$  ( $\bullet$ ),  $\alpha=0.95$  and  $\beta=1.00$  ( $\triangle$ ).

For  $\alpha = 0.01$  the probability of inserting a vehicle at the rightmost site of the left mini-system in two successive time step is very small and, therefore, the vehicles at the beginning of the system do not feel influence of each other. This means that a vehicle which is inserted at the rightmost site of the left mini system moves to  $i = 4$  at the next time step and can be found at site  $i = 4t$  after  $t$  times steps ( $t = 1, 2, 3, \dots$ ). The density on these sites is  $\rho \approx \alpha$  ( $\alpha \leq 0.1$ ).

For increasing injection rate  $\alpha$ , the probability of inserting a vehicle in two successive time steps increases which results in the increase in the hindrance that a vehicle feels from the front vehicle at the beginning of the system. This can be explained as follows [34]:

Suppose we insert a vehicle A in the mini-system at time step  $T$  and a vehicle at time step  $T + 1$ . Considering the system at time step  $T + 1$ , we see that vehicle A is on site  $i = 4$  and will move with velocity 4 where as vehicle B will occupy position  $i = 3$  in the next time step  $T + 2$  because the vehicles are inserted in left mini-system in such a way that the headway between the inserted vehicle and the next vehicle downstream is 4. At time  $T + t$ , vehicle A is on  $i = 4t$  and vehicle B is on  $i = 4(t - 1) - 1$ . In other words, we can say that the hindrance due to left boundary condition leads to a shift of the position of the vehicles within the system. This shift is reflected in the oscillation in the density profile of 8. The probability of finding a vehicle at  $i = 4t + 3$  is smaller than at  $i = 4t$  and it is much smaller for  $i = 4t + 2$  and even much smaller for  $i = 4t + 1$ .

As we move from the free flowing regime to congested flow regime (keeping  $\alpha$  fixed and decreasing  $\beta$ ) something interesting happens: the oscillations start vanishing and envelope of density profile rises (see Fig. 9). For low values of  $\beta$ , the density profile is just a constant whose value increases with decreasing  $\beta$ . This phenomenon is due to the hindrance that vehicles feel at the right boundary with decreasing probability



$\beta$ . Consequently a jam develops at the right boundary which expands to the left with decreasing  $\beta$ .

#### 4.2. Phase Diagram in the ADM

In order to identify the regions of free-flow and congested flow in the phase diagram of the ADM we measure the bulk density and the flux in the middle of the open system by varying the boundary rates and then compare it with the density and flux of the corresponding periodic system. Since density profile shows a periodic structure in the free flow regime, in order to compute the bulk density in the middle of the system, we average over the densities of  $V_{\max}$  lattice sites (i.e. one period of oscillation) for a given  $V_{\max}$ . The phase diagram of the ADM with open boundary conditions for  $V_{\max} = 4$  and  $V_{\max} = 9$  is shown in Fig. 10. The system will be found either in free-flow or congested-flow regime depending on the values of  $\alpha$  and  $\beta$ . Here, the  $\alpha = \beta$  line does not separate the free flowing and congested flow regime. Instead, the free flow regime is larger than the congested flow regime. The span of the free-flow regime increases with increasing  $V_{\max}$ . In the special case  $V_{\max} = 1$  the above insertion and extraction scheme leads us to the phase diagram of TASEP with open boundary and where the line  $\alpha = \beta$  separates free flow and congested flow regime.

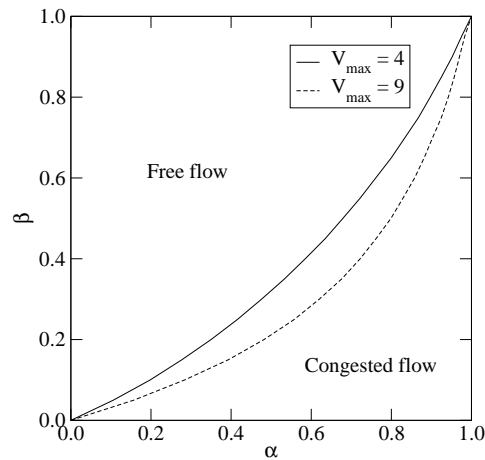


**Figure 10.** Phase diagram of aggressive driving model with open boundary conditions for  $V_{\max} = 4$  and  $V_{\max} = 9$ .

## 5. Cytoplasmic dynein: from experiment to model

In this section we first mention the main experimentally observed features of the steppings of dynein motors. Then, by extending the ADM, we develop a simple theoretical model that captures the essential features of dynein stepping.

### 5.1. Stepping of dynein: experimental results

In order to understand the mechanism of a single dynein motor, Mallik et al. [35] extracted the step size of single dynein motor from their experimental data. In their experiment, hindrance against forward movement of dyneins was caused by an opposing force. In principle, this hindrance could also be created by other motors. The smallest possible step size would be 8 nm as the equispaced binding sites on the microtubule form a lattice with lattice constant of 8 nm. Mallik et al. [35] observed that in the absence of hindrance the step sizes of dyneins were mostly  $\sim 32$  nm, i.e., four times the lattice constant. Moreover, the step size decreased with increasing hindrance: under weak hindrance the step size was approximately  $\sim 24$  nm, under intermediate hindrance step size was about  $\sim 16$  nm, whereas under strong hindrance dynein takes steps of  $\sim 8$  nm. On the basis of these observations, Mallik et al. [35] suggested a *molecular gear mechanism* for dynein motors.

In their generic model of molecular motor traffic, Parmeggiani et al. [15] implicitly assumed a hindrance-independent step size of the motors. Therefore, in the light of the experimental observations on dynein steppings [35], one may interpret the model developed in [15] to be a minimal model for the traffic of kinesin motors which are known to take steps of 8 nm irrespective of the hindrance. Therefore, to model the traffic of dynein motors, which can take steps of upto 32 nm (i.e., four times the lattice spacing in between the successive binding sites) at one go in the absence of hindrance, we need a more sophisticated model. In the next subsection we describe the model which we propose for the traffic of dynein motors.

### 5.2. Dynein traffic model (DTM)

Our dynein traffic model (DTM) has been obtained by extending the ADM which we have discussed extensively in the preceding sections. The lattice sites in this case represent the dynein binding site on the microtubule track and the lattice constant is 8 nm. In order to capture the fact that in the absence of hindrance a single dynein motor can take a single step of 32 nm, we set  $V_{\max} = 4$  in the ADM. Moreover, to capture the attachment and detachment of the motors from the microtubule track, we also allow the detachment of a motor from an occupied site with rate  $\omega_D$  and attachment of a motor to an empty site with rate  $\omega_A$ . The state of the system is updated in a random sequential manner. In this DTM, a single dynein motor can move forward by four lattice sites (i.e., 32 nm) in one single step if the available gap is greater than or equal to 32 nm; otherwise, the step size will be equal to the available gap as the mutual exclusion between the motors hinders the motion of the following dynein.

## 6. Results for DTM with periodic boundary conditions

In the case of periodic boundary condition we allow attachment and detachment of motors from all lattice sites with probability  $\omega_A$  and  $\omega_D$  respectively. Fig. 11 shows the

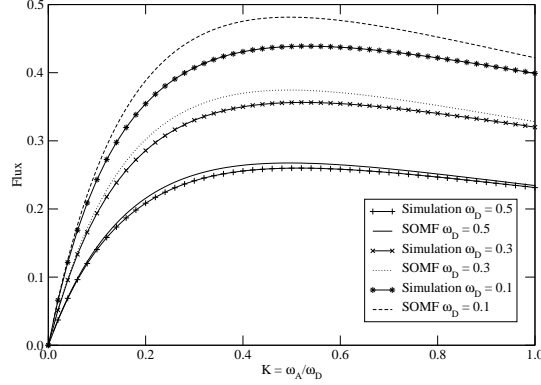


**Figure 11.** Flux  $f$  in the DTM for different values of the binding constant  $K$

values of flux  $f$  as a function of the binding constant  $K = \omega_A/\omega_D$  for different values of  $\omega_D$  obtained from the computer simulations. The flux initially increases with increasing  $K$  however after a threshold value of  $K$  it starts decreasing with the ratio  $K$ . In order to predict this variation theoretically we have carried out a Site-Oriented Mean Field (SOMF) calculation for the DTM following the same procedure as we followed earlier for the ADM. For  $V_{\max} = 4$ , we get

$$c_0(i, t + 1) = c(i + 1, t)[c_1(i, t) + c_2(i, t) + c_3(i, t) + c_4(i, t)] \quad (34)$$

$$c_1(i, t + 1) = qc(i + 1, t)d(i, t)c(i - 1, t) \quad (35)$$

$$c_2(i, t + 1) = qc(i + 1, t)d(i - 1, t)d(i, t)c(i - 2, t) \quad (36)$$

$$c_3(i, t + 1) = qc(i + 1, t)d(i - 2, t)d(i - 1, t)d(i, t)c(i - 3, t) \quad (37)$$

$$c_4(i, t + 1) = qd(i - 3, t)d(i - 2, t)d(i - 1, t)d(i, t)c(i - 4, t) \quad (38)$$

In the steady state, i.e.  $t \rightarrow \infty$ ,  $c_V(i, t)$  are independent of  $t$ . For periodic boundary conditions the system becomes homogeneous in the steady state and hence the  $i$ -dependence of  $c_V(i)$  also drops out. Therefore the steady state flux for  $V_{\max} = 4$  is given by

$$f = c_1 + 2c_2 + 3c_3 + 4c_4 = qcd[c + 2cd + 3cd^2 + 4d^3] \quad (39)$$

where  $q$  is the probability that the motor does, indeed, hop, instead of getting detached from the track. Finally, substituting  $q = 1 - \omega_D$ , the steady flux in the DTM, under the SOMF approximation, is given by

$$f = cd((1 - \omega_D)c + 2(1 - \omega_D)cd + 3(1 - \omega_D)cd^2 + 4(1 - \omega_D)d^3) \quad (40)$$

where  $c$  is given by the well-know ratio  $K/(1 + K)$  of Langmuir equilibrium density and  $d = 1 - c$ . In Fig. 11 we have shown the curves obtained from Eq. (40) along with the corresponding results from computer simulations. The results obtained from the SOMF theory show a good agreement with the simulation for high values of the detachment probability.

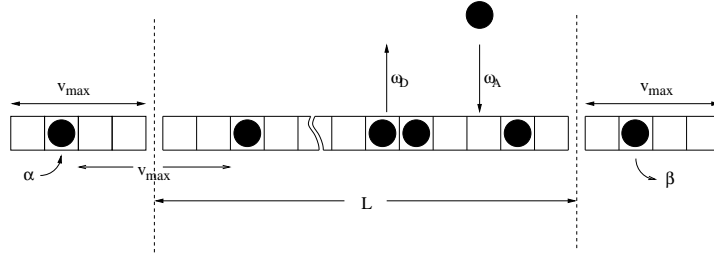


**Figure 12.** Schematic representation of the DTM with open boundary conditions.

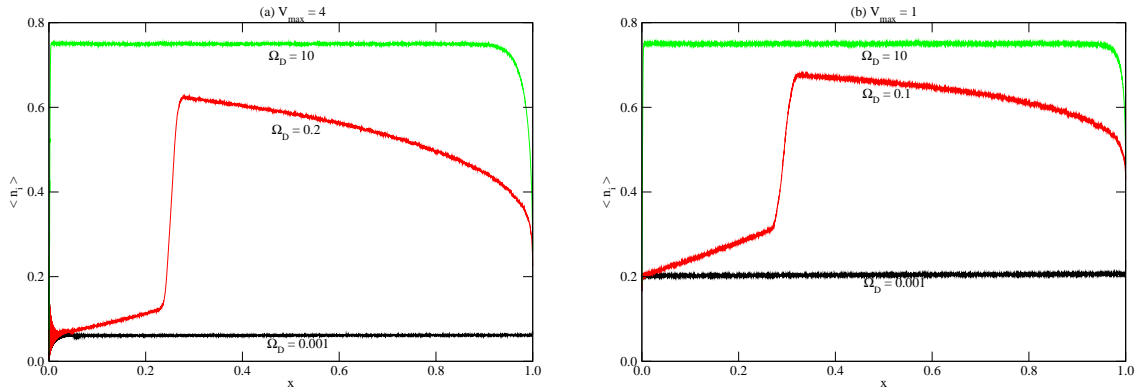


**Figure 13.** Average density profiles  $\langle n_i \rangle$  in the DTM obtained from Monte Carlo simulations and plotted against the rescaled space variable  $x = i/L$  for different values of  $\Omega_D$ . The common parameter values are  $L = 10000$ ,  $\alpha = 0.2$ ,  $\beta = 0.6$ ,  $K = 3$ .

## 7. DTM with open boundary condition

A schematic representation of the analysed system with open boundary conditions is given in Fig. 12. To capture the attachment and detachment of the motors from the microtubule we allow the detachment of a motor from an occupied site with rate  $\omega_D$  and attachment of a motor to an empty site with rate  $\omega_A$  in the bulk i.e. from all site other except those who belong to the reservoirs at the left and right boundary. Our proposed model with open boundary conditions reduced to the model of Parmeggiani et al. [15], which is a minimal model for the intra-cellular traffic of kinesin motors, if one sets  $V_{\max} = 1$ .

A competition between bulk dynamics (Langmuir kinetics) and boundary induced non-equilibrium effects (TASEP-like dynamics) is expected only if the particles injected either at boundary or somewhere in bulk visits a finite fraction of the total system size. In that case particles will spend enough time on lattice to feel mutual influence and eventually would produce collective effects.

Study of competition between bulk and boundary dynamics for large systems ( $L \gg 1$ ) requires that the kinetic rates  $\omega_A$  and  $\omega_D$  decrease simultaneously with

increasing system size  $L$ . This can be illustrated by considering the following heuristic argument given in ref. [15]. The average time  $\tau$  spent by a particle before detachment is roughly of the order of  $\sim 1/\omega_D$ . During this time  $\tau$  the number of sites  $n$  visited by a given particle is of the order of  $n \sim \tau$ . Therefore the fraction  $n/L$  ( $= 1/\omega_D L$ ) of the lattice site visited by a given particle during this time would tend to zero for fixed  $\omega_D$  as  $L \rightarrow \infty$ . In order that a given particles explores a finite fraction of the total sites before detaching for system size  $L \gg 1$ , one has to define the “total” detachment rate  $\Omega_D = \omega_D L$  such that  $\Omega_D$  remain constant as  $L \rightarrow \infty$ . A similar argument shows that a vacancy visits a finite fraction lattice sites until it is filled by the attachment of a particle if  $\omega_A$  scales to zero as  $\Omega_A/L$  with fixed “total” detachment rate  $\Omega_A$  [15]. Therefore we define total detachment rate  $\Omega_D = \omega_D L$  and total attachment rate  $\Omega_A = \omega_A L$  such that  $\Omega_D$  and  $\Omega_A$  remain constant as  $L \rightarrow \infty$ . Note that the binding constant  $K = \omega_A/\omega_D$  remains unchanged as  $L \rightarrow \infty$ .

### 7.1. Density profiles in the DTM

**7.1.1. Density profiles** In Fig. 13 (a) we have plotted the typical average density profiles  $\langle n_i \rangle$  obtained from Monte Carlo simulations for this model in rescaled space variable  $x = i/L$  (where  $n_i$  denotes occupation of  $n$ th lattice site in the bulk i.e.  $i = 1, 2, \dots, L$ ) by choosing a path in the parameter space along the curves with fixed  $\alpha, \beta$  and  $K$  while increasing  $\Omega_D = \Omega_A/K$ . For low values of kinetic rates  $\Omega_D, \Omega_A \ll \alpha, \beta$  the system remain in low-density phase where average density in the bulk remains constant. For High values of kinetic rates  $\Omega_D$  and  $\Omega_A$  the system goes to high density phase where average density in the bulk again constant. The bulk density in this case is determined by the well know ratio  $K/(1 + K)$  of Langmuir equilibrium density. For intermediate values of the rates, for example  $\Omega_D = 0.2$ , the density profile in the bulk exhibits unusual feature where regions of high density and low density are connected by a steep rise. In Fig. 13 (b) we have shown the density profiles obtained by Parmeggiani et al. [15] for their model where  $V_{\max} = 1$ . Comparison of Figs. 13 (a) and 13 (b) shows that the average bulk density in the low density phase in Fig. 13 (a) is smaller than in Fig. 13 (b). This observed decrease in the bulk density in the low density phase for identical values of the parameters  $\alpha, \beta, K$  and  $\Omega_D$  is due to the fact that particles in low density phase move with higher velocity which leads to higher current and lower density. Fig. 13 (a) also shows oscillations in the density profile at the beginning of the system in the low density phase. These oscillations result from the hindrance that particles have at the beginning of the system from each other [36]. These oscillations die out for higher systems sites. Comparison of Fig. 13 (a) and Fig. 13 (b) also shows that in the case of dynein motors the domain wall is found inside the the system for slightly higher value of  $\Omega_D$ .

Figure 14 shows the average density profile  $\langle n_i \rangle$  computed from Monte Carlo simulation in rescaled space variable  $x$  for different system sizes. The width of the transition region decreases with increasing system size. The data obtained from our

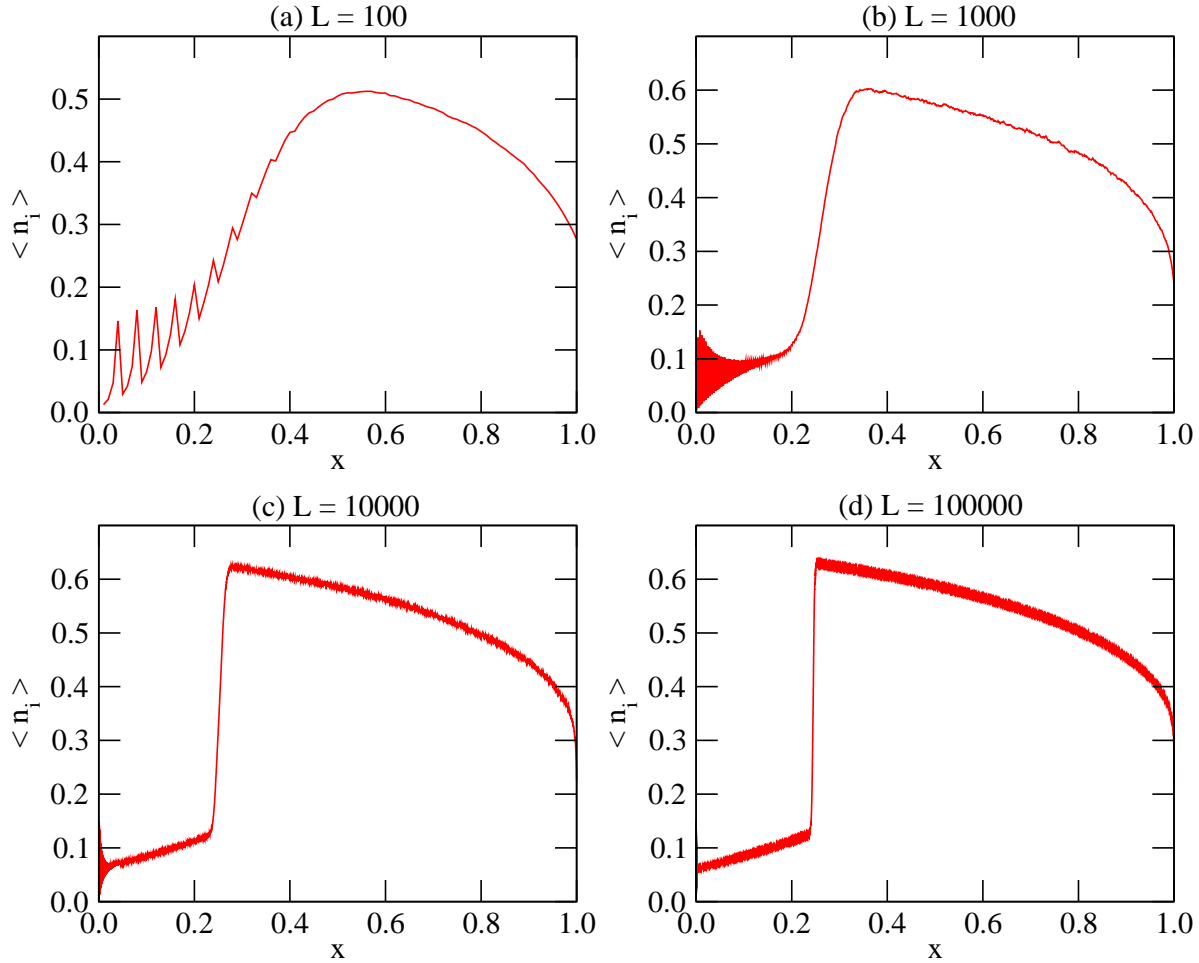


**Figure 14.** Average density profiles in the DTM obtained from Monte Carlo simulations and plotted against rescaled space variable for different system sizes. The common parameter values are  $\alpha = 0.2$ ,  $\beta = 0.6$ ,  $K = 3$  and  $\Omega_D = 0.2$ .

simulations suggest a sharp discontinuity of the density profile in terms of the rescaled space variable  $x = i/L$  in the limit  $L \rightarrow \infty$ . Therefore the low and high density phases separated by a sharp domain wall coexist in our model over an intermediate range of parameter values where boundary and bulk kinetic rates compete against each other. This discontinuity in the density profile is stable and the position of the domain wall is determined by the values of the kinetic rates as shown in Fig. 15. This coexistence of high and low density phase separated by a domain wall can be regarded as a *traffic jam* for molecular motors.

## 7.2. Phase diagrams in the DTM

In order to identify the regions of coexistence, we have obtained the phase diagram of our model for intra-cellular traffic of dynein motors by varying the boundary rates  $\alpha$  and  $\beta$  for fixed values of  $K$  and  $\Omega_D$ . Fig. 16(a) shows the phase diagram for  $\Omega_D = 0$ . In this

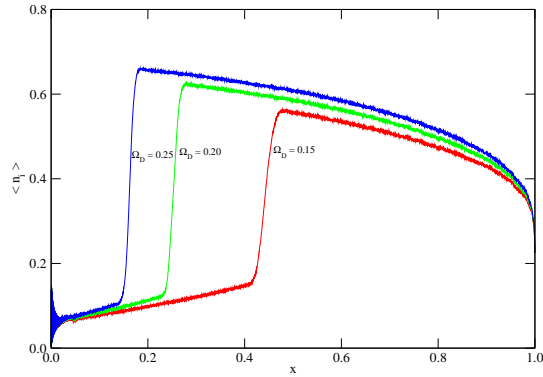


**Figure 15.** Domain wall positions in the DTM for different values of  $\Omega_D$ . The common parameter values are  $L = 10000$ ,  $\alpha = 0.2$ ,  $\beta = 0.6$  and  $K = 3$ .

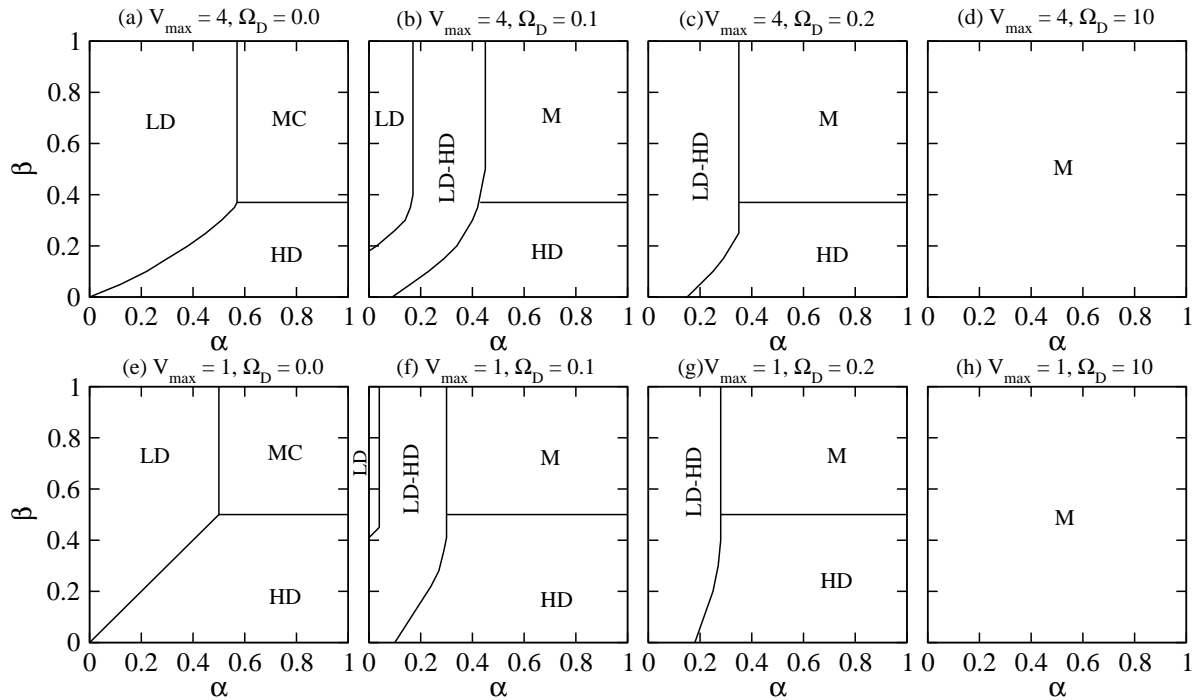


**Figure 16.** Phase diagrams of the DTM for (a)  $V_{\max} = 4, \Omega_D = 0.0$  (b)  $V_{\max} = 4, \Omega_D = 0.1$  (c)  $V_{\max} = 4, \Omega_D = 0.2$  and (d)  $V_{\max} = 4, \Omega_D = 10$  (e)  $V_{\max} = 1, \Omega_D = 0.0$  (f)  $V_{\max} = 1, \Omega_D = 0.1$  (g)  $V_{\max} = 1, \Omega_D = 0.2$  and (h)  $V_{\max} = 1, \Omega_D = 10$ . Other common parameter values are  $L = 10000$ ,  $K = 3$ .

case model reduces to the aggressive driving model with random sequential updating. For  $\Omega_D = 0$ , by varying boundary rates  $\alpha$  and  $\beta$  one gets three kind of phases namely Low density phase (LD), High density phase (HD) and Maximal Current phase (MC). For very small values of  $\Omega_D$  ( $\Omega_D \sim 0.001$ ) the boundary rates  $\alpha$  and  $\beta$  dominate and the structure of the phase diagram is determined only by the boundary rates  $\alpha$  and  $\beta$ . For  $\Omega_D \sim 0.001$  one obtained a phase digram similar to Fig. 16(a). On increasing the value of  $\Omega_D$  the boundary and bulk rates start competing with each other and in this case one gets a phase diagram where MC phase disappears and one can identify four distinct regions in the phase diagram namely, Low density phase (LD), Low density high density coexistence region (LD-HD), High density phase (HD) and “Meissner” (M) phase. The Meissner phase [15] has some interesting features that are genuinely distinct from the High density phase. The density profile in the bulk is independent of the boundary rates  $\alpha$  and  $\beta$  and is determined only by the bulk. On further increase of  $\Omega_D$  the low density phase also disappears from the phase diagram as shown in Fig. 16(c) and in this case one gets HD phase, M phase and coexistence region. For large values of  $\Omega_D$  the phase diagram is spanned only by the M phase as shown in Fig. 16 (d). In Fig. 16(e)-(h) we have shown phase diagrams of the model of Parmeggiani et al. [15] for the identical set of parameters. Comparison of the phase diagrams shown in Figs. 16(a)-(d) and 16(e)-(h) shows that the regions of coexistence of Low and High density phases are slightly different in the  $\alpha - \beta$  plane for identical values of the parameters  $K$  and  $\Omega_D$ .

### 7.3. Transportation efficiency

Comparison of 32 nm step of dynein at in the absence of hindrance and 8 nm step of kinesin implies that as a cargo transporter the dynein is four times more fuel-efficient than kinesin as both require one molecule of ATP as fuel. To study the transportation efficiency of dynein motors and kinesin motors as a function of the parameters  $K$  and  $\Omega_D$  we define the transportation efficiency by the relation

$$\% \text{Transportation efficiency} = \frac{\text{No. of steps taken}}{\text{No. of attempts made} \times 4} \times 100 \quad (41)$$

The above relation has been defined in such a way that if a dynein motor takes 4 steps of 8 nm in each attempt (i.e. for each ATP hydrolysis) then its efficiency will be 100 % similarly if a kinesin motor takes 1 step of 8 nm in each attempt then its efficiency will be equal to 25 %. The transportation efficiency of cytoplasmic dynein motors ( $V_{\max} = 4$ ) and kinesin motors ( $V_{\max} = 1$ ) are plotted in Fig. 17 (a) and Fig. 17 (b) for different values of  $\Omega_D$  and  $K$ . There is practically no difference between the efficiency of dynein and kinesin motors for very large values of  $\Omega_D$  and  $K$  ( $\Omega_D \sim 10$  and  $K \sim 10$ ) as for very large values of  $\Omega_D$  and  $K$  system is found in high density phase (HD).



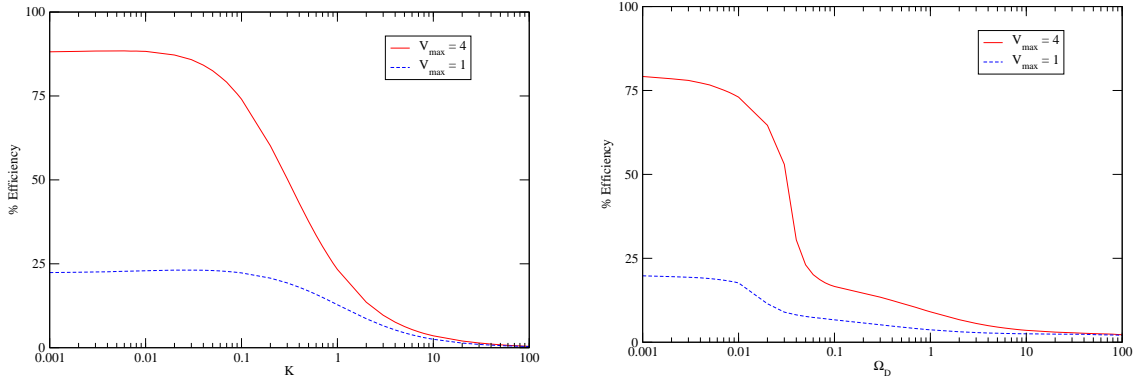


**Figure 17.** Efficiency of dynein and kinesin motors for (a) different values of  $K$  and (b)  $\Omega_D$ . The common parameter values are  $L = 1000$ ,  $\alpha = 0.2$  and  $\beta = 0.6$

## 8. Summary and conclusions

In this paper we have first investigated the properties of the aggressive driving model (ADM) which is a simple cellular automata model for vehicular traffic. One of the motivations for considering this model is that the rule for aggressive driving can be naturally extended to capture the special features of step sizes of dynein motors and, therefore, the ADM is ideally suited for extending so as to study intra-cellular molecular motor traffic by dynein motors.

The ADM shows different behavior for  $V_{\max} = 1$  and  $V_{\max} > 1$ . For  $V_{\max} = 1$  the model is identical to the NaSch model with  $V_{\max} = 1$  which has perfect particle-hole symmetry. This symmetry is broken for  $V_{\max} > 1$ . The fundamental diagram of this model in the special limit  $V_{\max} = \infty$  has a form which is quite different from that of the NaSch model in the limit  $V_{\max} = \infty$ . We have also shown few distance headway and time-headway distributions. We have calculated the fundamental diagram using two different mean-field approaches, namely, site-oriented mean-field approach (SOMF) and car-oriented mean-field approach (COMF). A simple SOMF theory shows a poor agreement with the simulation data. However, an improved mean field theory, namely COMF, shows good agreement with the numerical data obtained from computer simulations. We compare our ADM with the Nagel-Schreckenberg model which captures essential features of normal driving. We have also investigated the density profiles and phase diagrams of this model replacing the periodic boundary conditions by open boundary conditions. The density profile of this model with open boundary conditions shows periodic structures in the free-flowing regime whose period of oscillation depends on the maximum attainable velocity  $V_{\max}$ .

We have extended the ADM to develop a dynein traffic model (DTM) which is a model of intra-cellular molecular motor traffic from cell periphery towards the nucleus of the cell. We have investigated the properties of this model with periodic and open boundary conditions. Under open boundary conditions, DTM shows an unusual feature where low and high density phases separated by a static domain wall coexist over a

range of parameter values which can be interpreted as a traffic jam of molecular motors. This is in sharp contrast to the phase diagram of the ADM which does not exhibit such coexistence of congested and free-flowing regions. The occurrence of the phase is, thus intimately related to the competition between the hopping and the kinetics of attachment/detachment of the motors on the track. Finally, we have compared the efficiencies of dynein and kinesin motors for different values of parameters. For very large values of the parameters  $\Omega_D$  and  $K$  system is found in the high density phase and, in that case, one observes practically no difference between the efficiencies of kinesin and dynein motors.

To our knowledge, our DTM is the first model of traffic-like collective transport of *dynein* motors on filamentary microtubule tracks. A model that incorporates both the species of dyneins and kinesin motors, which move in opposite directions along the same track, may provide deep insight into experimentally observed bidirectional traffic [37].

**Acknowledgements:** This work has been supported (through DC), in part, by the Council of Scientific and Industrial Research (CSIR) of the government of India. DC also thanks Max-Planck Institute for Physics of Complex Systems, Dresden, for hospitality during a short visit when a part of this manuscript was prepared.

## References

- [1] M. Schliwa (ed.), *Molecular Motors*, (Wiley-VCH, 2003).
- [2] J. Howard, *Mechanics of Motor Proteins and the Cytoskeleton* (Sinauer Associates, Massachusetts, 2001).
- [3] D. Chowdhury, A. Schadschneider, K. Nishinari, Phys. Life Rev. **2**, 318 (2005)
- [4] See the special issue of Physica A (2006) for the close similarities and crucial differences between biological traffic and vehicular traffic.
- [5] Physica Scripta (*Royal Swedish Academy of Sciences*), **T106**, 13 (2003).
- [6] D. Chowdhury, L. Santen, and A. Schadschneider, Phys. Rep. **329**, 199 (2000).
- [7] B. Schmittmann and R.K.P. Zia, in: *Phase Transition and Critical Phenomena*, Vol. 17, eds. C. Domb and J. L. Lebowitz (Academic Press, 1995).
- [8] G. Schütz, in: *Phase Transition and Critical Phenomena*, Vol. 19, eds. C. Domb and J. L. Lebowitz (Academic Press, 2000).
- [9] V. Privman (ed.), *Nonequilibrium Statistical Mechanics in One Dimension* (Cambridge University Press, 1997)
- [10] J. Marro and R. Dickman, *Nonequilibrium Phase Transitions in Lattice models*, (Cambridge University Press, 1999)
- [11] S. Wolfram, *Theory and Applications of Cellular Automata* (World Sci., 1986); *A New Kind of Science* (Wolfram Research Inc., 2002)
- [12] C. MacDonald, J. Gibbs and A. Pipkin, Biopolymers, **6**, 1 (1968).
- [13] C. MacDonald and J. Gibbs, Biopolymers, **7**, 707 (1969).
- [14] B. Derrida, Phys. Rep. **301**, 65 (1998).
- [15] A. Parmeggiani, T. Franosch and E. Frey, Phys. Rev. Lett. **90**, 086601 (2003); Phys. Rev. E **70**, 046101 (2004).
- [16] E. Frey, A. Parmeggiani and T. Franosch, Genome Inf. **15**, 46 (2004) and references therein.
- [17] R. Lipowsky, S. Klumpp and T.M. Nieuwenhuizen, Phys. Rev. Lett. **87**, 108101 (2001).

- [18] R. Lipowsky and S. Klumpp, *Physica A* **352** 53 (2005) and references therein; R. Lipowsky, Y. Chai, S. Klumpp, S. Liepelt and M. J. I. Müller, in [4] and references therein.
- [19] M.R. Evans, R. Juhasz and L. Santen, *Phys. Rev. E* **68**, 026117 (2003).
- [20] V. Popkov, A. Rakos, R.D. Williams, A.B. Kolomeisky and G.M. Schütz, *Phys. Rev. E* **67**, 066117 (2003).
- [21] A. Schadschneider, in: *Traffic and Granular Flow '97*, ed. by M. Schreckenberg and D.E. Wolf (Springer, 1998)
- [22] K. Nagel and M. Schreckenberg, *J. Physique I* **2**, 2221 (1992)
- [23] M. Schreckenberg, A. Schadschneider, K. Nagel and N. Ito, *Phys. Rev. E* **51**, 2939 (1995); A. Schadschneider and M. Schreckenberg, *J. Phys. A* **26**, L679 (1993)
- [24] M. Fukui, Y. Ishibashi, *J. Phys. Soc. Jpn.*, **65**, 1868 (1996)
- [25] A. Schadschneider, *Physica A* **313**, 153 (2002)
- [26] K. Ghosh, A. Majumdar, D. Chowdhury, *Phys. Rev. E* **58**, 4012 (1998)
- [27] K. Nagel and H. J. Herrmann, *Physica A* **199**, 254 (1993)
- [28] M. Sasvári and J. Kertész, *Phys. Rev. E* **56**, 4104 (1997)
- [29] Sascha Grabolus, diplom thesis, University of Cologne (2001)
- [30] B. H. Wang, Y. R. Kwong and P. M. Hui, *Phys. Rev. E* **57**, 2568 (1998); *Physica A* **254**, 122 (1998)
- [31] B. H. Wang, L. Wang, P.M. Hui and B. Hu, *Phys. Rev. E* **58**, 2876 (1998)
- [32] A. Schadschneider and M. Schreckenberg, *J. Phys. A* **30**, L69 (1997)
- [33] R. Barlovic, T. Huisinga, A. Schadschneider, and M. Schreckenberg, *Phys. Rev. E* **66**, 046113 (2002)
- [34] S. Cheybani, J. Kertész and M. Schreckenberg, *Phys. Rev E* **63**, 016107 (2000)
- [35] R. Mallik, B. C. Carter, S. A. Lex, S. J. King and S. P. Gross, *Nature* **427**, 649 (2004).
- [36] S. Cheybani, J. Kertész and M. Schreckenberg, *Phys. Rev E* **63**, 016108 (2000).
- [37] S.P. Gross, *Phys. Biol.* **1**, R1 (2004).